

Electron-Phonon Coupling in Boron-Doped Diamond Superconductor

H. J. Xiang, Zhenyu Li, Jinlong Yang,* J. G. Hou, and Qingshi Zhu

*Hefei National Laboratory for Physical Sciences at Microscale,
Laboratory of Bond Selective Chemistry and Structure Research Laboratory,
University of Science and Technology of China,
Hefei, Anhui 230026, People's Republic of China*

(Dated: October 30, 2019)

Abstract

The electronic structure, lattice dynamic, and electron-phonon coupling in the boron-doped diamond are investigated using density functional supercell calculations. Calculations of the electron-phonon coupling show that the optical phonon modes involving B vibrations provide most of the coupling. Our results indicate the boron-doped diamond is a phonon mediated superconductor, confirming previous theoretical conclusions deduced from the calculations employing the virtual crystal approximation. Different from previous theoretical results, from our study the electron-phonon coupling constant is 0.39 and the estimated superconducting transition temperature T_c is 2.7 K with the Coulomb pseudopotential $\mu^* = 0.12$ for the boron doped diamond with 2.78% boron content, in excellent agreement with experimental results. By using a more sophisticated model, we resolve the discrepancy between theoretical results based on the virtual crystal approximation and experimental data.

PACS numbers: 74.25.Kc,74.25.Jb,74.70.Ad,74.62.Dh

Recently, Ekimov *et al.* reported the discovery of superconductivity in the boron-doped diamond synthesized at high pressure and high temperature [1]. Their measurements showed that the boron-doped diamond with a hole carrier density of $5 \times 10^{21} \text{ cm}^{-3}$ is a bulk, type-II superconductor below the superconducting transition temperature $T_c \approx 4 \text{ K}$. Using McMillan formula [2], they estimated the electron-phonon coupling constant $\lambda = 0.2$, indicative of weak electron-phonon coupling.

Before that, a few superconducting semiconductors have been discovered experimentally: bulk superconductivity with $T_c \approx 0.1 - 0.5 \text{ K}$ was found in self-doped GeTe and SnTe at carrier densities $n \approx 10^{21} \text{ cm}^{-3}$, in doped SrTiO₃ ($T_c \approx 0.05 - 0.25 \text{ K}$ at $n \approx 10^{19} - 10^{21} \text{ cm}^{-3}$) [3], and in samples of TlBiTe₂ with nominal carrier densities of approximately 6×10^{20} holes per cm^3 [4]. Theoretically, Cohen predicted superconductivity in many-valley degenerate semiconductor [5]. As for the boron-doped diamond superconductor, Baskaran *et al.* [6] suggested a resonating valence bond (RVB) [7] mechanism of impurity band superconductivity in diamond. When the dopant boron concentration increases to a critical doping concentration $n_c \approx 4 \times 10^{21} / \text{cm}^3$, an Anderson-Mott insulator to RVB superconductivity transition takes place. Boeri and co-workers [8] substantiated by first principles density functional perturbation [9] calculations employing the virtual crystal approximation [10] that the recently discovered superconductivity below 4 K in 3% boron-doped diamond is caused by the coupling of a few holes at top of the σ -bonding valence band to the optical zone-center phonons, similar as in MgB₂ [11, 12, 13], albeit in 3 dimensions. Another first principles study employing the virtual crystal approximation and frozen phonon method indicated that the electron-phonon coupling strength $\lambda \approx 0.5$ leads to T_c in the 5 – 10 K range and makes electron-phonon coupling the likely mechanism [14]. Regardless of their similar conclusion that the large deformation potential of the hole states arising from the C-C bond stretch mode is responsible for the superconductivity in boron-doped diamond, but effects of three dimensionality keep doped diamond from having a T_c closer to that of MgB₂, we note that there are some disagreements in these two studies, especially the electron-phonon coupling strength and T_c : $\lambda = 0.27$ and $T_c = 0.2 \text{ K}$ when the Coulomb pseudopotential $\mu^* = 0.10$ for 3% doping concentration in the first study, however, $\lambda = 0.55$ and $T_c = 9 \text{ K}$ when $\mu^* = 0.15$ for 2.5% doping concentration in the second study. The difference in doping concentration results in even larger discrepancy since larger doping concentration leads to larger λ and T_c . Moreover, though qualitative agreement with experiment is found in these two studies,

some obvious disagreements still exist, in particular, T_c in the first study is too small, and T_c in the second study is too large though one can obtain $T_c = 4$ K by setting μ^* to some unrealistic value, i.e., 0.20. Since such large discrepancy exists, more theoretical works are desired. And whether the superconducting mechanism in the boron-doped diamond is RVB or conventional phonon mediated is unclear. In this paper, we report a first principles supercell calculation on the electron-phonon coupling of the boron-doped diamond to address some of these issues. Our results support the conventional phonon mediated superconducting mechanism in boron-doped diamond and the calculated T_c is in excellent agreement with experimental value.

Electronic structure calculations and geometrical optimizations are performed using density functional theory (DFT) [15, 16] in the local density approximation (LDA) [17, 18]. The electron-ion interaction is described by ultrasoft Vanderbilt-type pseudopotentials [19], allowing for a low cutoff energy (25 Ry in this work) in the plane-wave expansion. The phonon and electron-phonon coupling calculations are carried out using density functional perturbation theory in the linear response [9]. Within the electron-phonon mediated theory of superconductivity, T_c can be estimated using McMillan's solution of the Eliashberg equation [2],

$$T_c = \frac{\omega_{\text{ln}}^{\text{ph}}}{1.20} \exp \left\{ -\frac{1.04(1+\lambda)}{\lambda - \mu^*(1+0.62\lambda)} \right\}, \quad (1)$$

where λ is electron-phonon coupling constant, $\omega_{\text{ln}}^{\text{ph}}$ is a logarithmically averaged characteristic phonon frequency, and μ^* is the Coulomb pseudopotential which describes the effective electron-electron repulsion. The electron-phonon coupling λ is calculated as an average over the N \mathbf{q} -points mesh and over all the modes, $\lambda = \sum_{\mathbf{q}\nu} \lambda_{\mathbf{q}\nu} / N$, where $\lambda_{\mathbf{q}\nu}$ is the electron-phonon interaction for a phonon mode ν with momentum \mathbf{q} . The modes responsible for superconductivity can be identified from the Eliashberg function,

$$\alpha^2 F(\omega) = \frac{1}{2N} \sum_{\mathbf{q}\nu} \lambda_{\mathbf{q}\nu} \omega_{\mathbf{q}\nu} \delta(\omega - \omega_{\mathbf{q}\nu}). \quad (2)$$

Then $\omega_{\text{ln}}^{\text{ph}}$ is calculated as,

$$\omega_{\text{ln}}^{\text{ph}} = \exp \left\{ \frac{2}{\lambda} \int_0^\infty d\omega \alpha^2 F(\omega) \ln \omega / \omega \right\}. \quad (3)$$

We use the supercell technique to model the boron-doped diamond. In order to study the dependence of the electron-phonon coupling on the doping concentration, we choose two

models: $2 \times 2 \times 2$ and $3 \times 3 \times 2$ diamond supercells with a carbon atom substituted by a boron atom, named model I and II respectively. The total B content (C_B) for experimental samples is $2.8 \pm 0.5\%$, which is smaller than the total B content (6.25%) in model I and very close to the total B content (2.78%) in model II. The two models are shown in Fig 1. The optimized lattice constant for diamond is 3.57 \AA , agreed well with the experimental lattice constant [1] and previous theoretical results [20]. For the boron-doped diamond we check that our calculations reproduce the slight lattice expansion [1]. When increasing the hydrostatic pressure up to 8 Gpa, the lattice constant for the undoped and doped diamond decreases less than a few percents due to the large bulk modulus, which indicates hydrostatic pressure has little effect on the superconductivity transition temperature, consistent with experimental results [1]. Since the pressure and not very large boron doping have negligible effect on the lattice constant of diamond, we used the experimental lattice constant for the undoped materials in all subsequent calculations.

The k integration for geometrical optimization, the construction of the induced charge density and the dynamical matrix is performed over a $4 \times 4 \times 4$ ($2 \times 2 \times 3$) Monkhorst-Pack grid [21] for model I (II), and a larger $8 \times 8 \times 8$ ($4 \times 4 \times 6$) grid is used in the phonon linewidth calculations since the convergence in the k-point sampling for the phonon linewidth calculations is more difficult than that for the phonon calculations.

The total electronic density of states (EDOS) and local density of states (LDOS) for model I and II are plotted in Fig 2. The EDOS clearly indicates a degenerate or metallic behavior in both models. The EDOS and LDOS for model I are very similar with those for model II except that the energy difference between the valence top and the fermi level for model I is larger than that for model II. The width of the acceptor levels for model I is larger than that for model II, and both are larger than that for a boron-doped diamond 64-atom supercell, obtained by Barnardy *et al.* [22]. This suggests a dependence of the width of the acceptor levels on the boron doping concentration. When the doping concentration decreases, the width of the donor states decreases. At very small doping concentration, the donor states even no longer overlap with the valence band edge of the diamond resulting in a threefold degenerate acceptor state with a hole bind energy of $E_B \approx 0.37 \text{ eV}$ [23]. The metallization in the boron-doped diamond is reasonably caused by the increased boron content, doesn't necessarily resort to the Anderson s-d hybride model [24]. Fig 2(c) and (d) show the LDOS of the boron atom and one of the four C atoms nearest to B. The

LDOS for other C atoms differ only a little for the C LDOS shown here. Fig 2(c) and (d) clearly indicate that the LDOS for B mainly locates near fermi level and the LDOS around the Fermi level for B is larger than that for the selected C atom. The partial charge near the Fermi level also has a largest density around B though the charge density indicates a reduction in the electron density surrounding the boron atom. However, it doesn't mean the electronic states near the Fermi level are localized around B since the sum of the LDOS for all C atoms is a lot larger than the LDOS for B.

The calculated frequency of the highest Γ optical phonon for the updoped diamond is 1295 cm^{-1} , agreed well with previous LDA calculations [8, 20], a little smaller than experimental frequency, 1332 cm^{-1} [1]. The phonon band structures for the undoped and boron-doped $2 \times 2 \times 2$ supercell diamond are shown in Fig 3(a) and (b) respectively. Here, we plot the phonon band structure for the supercell diamond just for comparison with that for the boron-doped diamond. The phonon band structure for the supercell diamond is more complex than that for the unit cell diamond since there are much more carbon atoms in the supercell diamond. There are more lines for the boron-doped diamond since some phonon degenerates are removed due to the symmetry breaking. Beside that, a general effect to the phonon band structures resulting from the boron doping is the phonon softening. Especially the softening of the optical phonons is sizeable, e.g., the highest frequency of the zone center optical phonons decreases 99 cm^{-1} to 1196 cm^{-1} . We can see that there is a slight upturn of the uppermost mode especially when moving from Γ to X for both updoped and doped diamond, similar to the previous results [20, 25], moreover, the upturn for the boron-doped diamond is more noticeable possibly due to the larger electron-phonon coupling for the zone center optical phonons.

The phonon density of states (DOS) for both models are shown in the upper panels of Fig 4. The shapes of the phonon DOS for these two models are very similar except that the phonon softening effect is stronger in model I due to the larger boron concentration. The lower panels of Fig 4 are the Eliashberg function $\alpha^2 F(\omega)$ and the boron partial phonon DOS for both models. The extremely weak signal in the low frequency part (lower than 80 meV) of $\alpha^2 F(\omega)$ indicates very weak electron acoustic phonon coupling. The strongest peak of $\alpha^2 F(\omega)$ for model I doesn't correspond to that of the total phonon DOS, but near the strongest peak for the boron partial phonon DOS. For model II, a strong double peak is prominent in $\alpha^2 F(\omega)$ with a peak corresponding to the peak of the total phonon DOS.

The large similarity in shape between the boron partial phonon DOS and $\alpha^2F(\omega)$ suggests the significant role of the boron vibrations in the electron-phonon coupling. This doesn't mean that only boron vibrations contribute to the electron-phonon coupling since all the vibrational modes are delocalized and no localized boron vibration exists due to the little mass difference between boron and carbon. Comparing our calculated $\alpha^2F(\omega)$ with those obtained by Boeri *et al.*, we find that $\alpha^2F(\omega)$ has sizeable contributions from phonons with medium frequency in our results, however, $\alpha^2F(\omega)$ vanishes for phonon frequencies below that of the optical zone-center modes, then jumps to a maximum, and finally falls in their results [8]. Their relative simple picture for $\alpha^2F(\omega)$ should stem from the fact that there are only three optical phonon modes in their virtual crystal calculations. Since we involve much more phonon modes to calculate $\alpha^2F(\omega)$, our results should be more reliable.

The calculated DOS at the Fermi level ($N(E_F)$), average frequencies $\omega_{\text{ln}}^{\text{ph}}$, electron-phonon coupling constants λ , and superconducting transition temperatures T_c for model I and II are listed in Table I. As expected, the $N(E_F)$ for model I is larger than that for model II due to the larger boron concentration. The $N(E_F)$ for the boron-doped diamond agrees well with the virtual crystal calculations: $N(E_F)$ (in states/(spin · eV · diamond unit cell)) is 0.062 for 2.78% boron vs 0.060 for 2.5% boron [14], 0.106 for 6.25% boron vs 0.08 for 5% boron [8]. The smaller $N(E_F)$ for the boron-doped diamond than MgB₂ would result in weaker electron-phonon coupling in the boron-doped diamond. The large $\omega_{\text{ln}}^{\text{ph}}$ for the boron-doped diamond leads to high T_c , as demonstrated in McMillan's formula. Though the phonon softening increases with increased boron concentration, $\omega_{\text{ln}}^{\text{ph}}$ for model I is larger than that for model II, 1287 K vs 1218 K. The smaller $\omega_{\text{ln}}^{\text{ph}}$ for model II results from the substantial electron-phonon coupling in the medium frequency region. The electron-phonon coupling constants λ for model I is 0.56, larger than that for model II with $\lambda = 0.39$. The typical value for μ^* is in the range 0.12 to 0.14. The calculated T_c for model I is 18.2 (13.5) K for $\mu^* = 0.12$ (0.14), and for model II it is 2.7 (1.3) K for $\mu^* = 0.12$ (0.14). The boron concentration for model II is very close to the experimental value and the calculated T_c agrees well with experimental T_c , about 4 K. We can see T_c increases with increased boron concentration due to the increased λ . Detailed analysis reveals that the Γ phonons contribute more to the electron-phonon coupling than other phonons, which is also found in previous study [8]. The relative large λ and T_c obtained by Lee *et al.* [14] might result from the fact that their frozen phonon calculations only took into account the Γ only phonons,

but sampling the whole Brillouin zone (BZ) is required since the electron-phonon coupling constant λ is averaged over the whole BZ.

Our treatment neglects the anharmonic corrections, which is well known to harden the optical phonon modes and thus decrease λ , e.g., λ is decreased from 1.0 to 0.78 in MgB_2 [13]. Boeri *et al.* considered the anharmonic corrections in the boron-doped diamond using frozen phonon calculations and found the effect of anharmonicity is small, i.e., in general λ decreases 0.03 after taking into account the anharmonicity [8]. So our main results remain essentially unchanged even after including the anharmonic corrections.

In summary, we have carried out a first principles study on the heavily boron-doped diamond. Optical phonons in diamond are softened after doped with boron. The Eliashberg function $\alpha^2F(\omega)$ is mainly contributed by the boron related vibrational modes. Superconductivity in the boron-doped diamond is found to be mediated by the electron-phonon coupling. By using the supercell technique, we resolve the discrepancy between theoretical results based on the virtual crystal approximation and experimental data, and the calculated T_c is in excellent agreement with experimental results.

This work is partially supported by the National Project for the Development of Key Fundamental Sciences in China (G1999075305, G2001CB3095), by the National Natural Science Foundation of China (50121202, 20025309, 10074058), by the Foundation of Ministry of Education of China, by the Foundation of the Chinese Academy of Science, and by the USTC-HP HPC project.

* Corresponding author. E-mail: jlyang@ustc.edu.cn

- [1] E. A. Ekimov, V. A. Sidorov, E. D. Bauer, N. N. Mel'nik, N. J. Curro, J. D. Thompson, and S. M. Stishov, *Nature (London)* **428**, 542 (2004).
- [2] W. L. McMillan, *Phys. Rev.* **167**, 331 (1968).
- [3] J. F. Schooley, W. R. Hosler, and M. L. Cohen, *Phys. Rev. Lett.* **12**, 474 (1964).
- [4] R. A. Hein and E. M. Swiggard *Phys. Rev. Lett.* **24**, 53 (1970).
- [5] M. L. Cohen, *Phys. Rev.* **134**, A511 (1964).
- [6] G. Baskaran, cond-mat/0404286.
- [7] P. W. Anderson, *Science* **235**, 1196 (1987).

- [8] L. Boeri, J. Kortus, and O. K. Andersen, cond-mat/0404447.
- [9] S. Baroni, S. de Gironcoli, A. Dal Corso, and P. Giannozzi, Rev. Mod. Phys. **73**, 515 (2001);
S. Baroni, A. Dal Corso, S. de Gironcoli, and P. Giannozzi, <http://www.pwscf.org>.
- [10] L. Nordheim, Ann. Phys. (Leipzig) **9**, 607 (1931).
- [11] J. Nagamatsu, N. Nakagawa, T. Muranaka, Y. Zenitani and J. Akimitsu, Nature (London) **410**, 63 (2001).
- [12] J. M. An, W. E. Pickett, Phys. Rev. Lett. **86**, 4366 (2001).
- [13] H. J. Choi, D. Roundy, H. Sun, M. L. Cohen, S. G. Louie, Nature (London) **418** 758 (2002);
Phys. Rev. B **66**, 020513(R) (2002).
- [14] K.-W. Lee, W. E. Pickett, cond-mat/0404547.
- [15] P. Hohenberg and W. Kohn, Phys. Rev. **136**, B864 (1964).
- [16] W. Kohn and L. J. Sham, Phys. Rev. **140**, A1133 (1965).
- [17] D. M. Ceperley and B. J. Alder, Phys. Rev. Lett. **45**, 566(1980).
- [18] J. P. Perdew and A. Zunger, Phys. Rev. B **23**, 5048 (1981).
- [19] D. Vanderbilt, Phys. Rev. B **41**, 7892 (1990).
- [20] N. Vast and S. Baroni, Phys. Rev. B **61**, 9387 (2000).
- [21] H. J. Monkhorst and J.D. Pack, Phys. Rev. B **13**, 5188 (1976).
- [22] A. S. Barnardy, S. P. Russoz, and I. K. Snook, Philos. Mag. **83**, 1163 (2003).
- [23] F. Fontaine, J. Appl. Phys. **85**,1409 (1999).
- [24] Yu. G. Pogorelov and V. M. Loktev, cond-mat/0405040.
- [25] M. Schwoerer-Böhning, A. T. Macrander, and D. A. Arms, Phys. Rev. Lett. **80**, 5572 (1998).

TABLE I: Computed electronic DOS at the Fermi level ($N(E_F)$), average frequencies ω_{ln}^{ph} , electron-phonon coupling constants λ , and superconducting transition temperatures T_c for model I and II. The two values for T_c correspond to two different values of μ^* (0.12 and 0.14). $N(E_F)$ is in states/(spin \cdot eV \cdot diamond unit cell). Boron content C_B is also shown for each model.

	C_B	$N(E_F)$	ω_{ln}^{ph} (K)	λ	T_c (K)
Model I	6.25%	0.106	1287	0.56	18.2,13.5
Model II	2.78%	0.062	1218	0.39	2.7,1.3

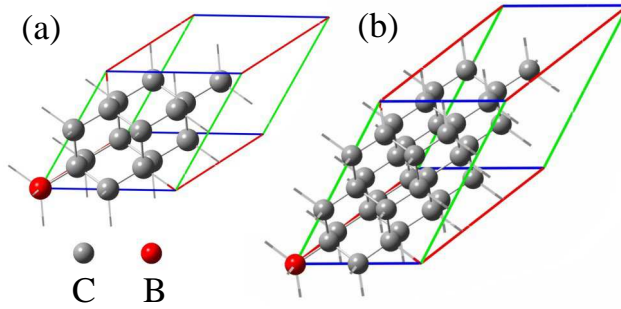


FIG. 1: Structures of (a) model I and (b) model II. Refer to the text for the description for model I and II.

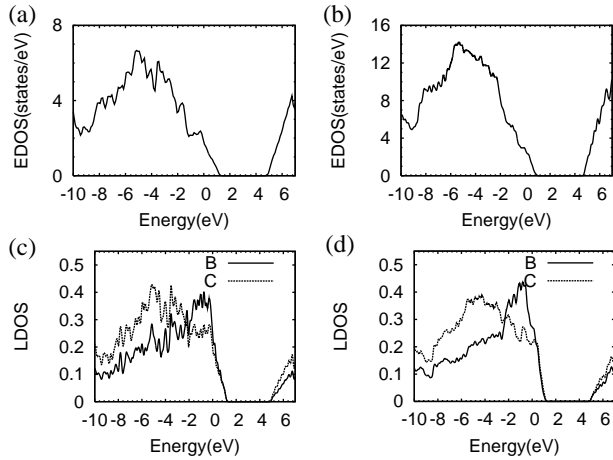


FIG. 2: Total EDOS and LDOS for model I and II. (a) and (b) are the EDOS plots for model I and II. (c) and (d) are the LDOS plots for model I and II. The LDOS for C shown here represents the LDOS of one of the C atoms nearest to B.

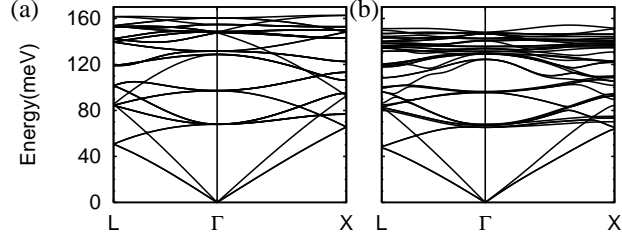


FIG. 3: Phonon band structures for (a) $2 \times 2 \times 2$ supercell diamond and (b) $2 \times 2 \times 2$ supercell diamond with a carbon atom substituted by a boron atom (model I).

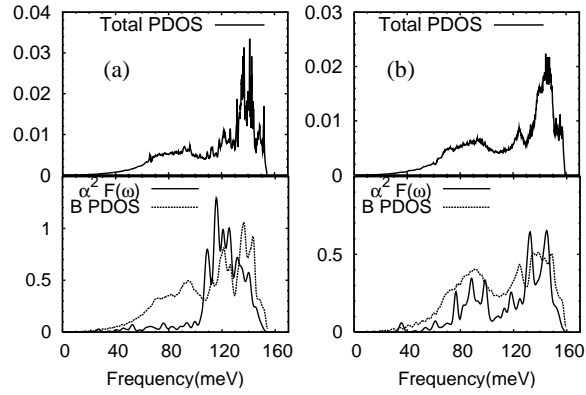


FIG. 4: Total phonon DOS, Eliashberg function $\alpha^2 F(\omega)$, and boron partial phonon DOS for (a) model I and (b) model II. Boron partial phonon DOS shown here is in arb. units.